INORGANIC CHEMISTRY FRONTIERS

CCS 中国化学会 CHINESE CHEMICAL SOCIETY

ROYAL SOCIETY OF CHEMISTRY

High Proton Conductivity in Nb^{5+}-doped $BaScO_{2.5}$

Journal:	*Inorganic Chemistry Frontiers*
Manuscript ID	QI-RES-03-2025-000632.R1
Article Type:	Research Article
Date Submitted by the Author:	18-May-2025
Complete List of Authors:	Saito, Kei; Tokyo Institute of Technology, Chemistry Baba, Mitsuki; Institute of Science Tokyo Umeda, Kensei; Tokyo Institute of Technology, Chemistry Fujii, Kotaro; Tokyo Institute of Technology, Honda, Takashi; High Energy Accelerator Research Organization (KEK), Institute of Materials Structure Science Yashima, Masatomo; Tokyo Institute of Technology, Chemistry

ARTICLE

High Proton Conductivity in Nb^{5+}-doped $BaScO_{2.5}$

Kei Saito,[a] Mitsuki Baba,[a] Kensei Umeda,[a] Kotaro Fujii,[a] Takashi Honda,[b,c] Masatomo Yashima[a,*]

Received 00th January 20xx,
Accepted 00th January 20xx

DOI: 10.1039/x0xx00000x

Ceramic proton conductors are promising materials for clean energy. In contrast to the conventional acceptor doping, donor doping into the oxides with intrinsic oxygen vacancies is a novel strategy to achieve the reduced proton trapping. Here, we report high proton conductivity (e.g., 0.01 S cm^{-1} at 320 °C) and high chemical stability of pentavalent donor doped $BaScO_{2.5}$, $BaSc_{0.75}Nb_{0.25}O_{2.75}$. The high proton conductivity is attributable to high proton concentration and high proton diffusion coefficient. The high proton concentration is ascribed to a large amount of oxygen vacancies in $BaSc_{0.75}Nb_{0.25}O_{2.75}$ and full hydration in hydrated $BaSc_{0.75}Nb_{0.25}O_{2.75}$. The high proton diffusion coefficient is attributable to its low activation energy, suggesting reduced proton trapping due to the repulsion between the donor Nb^{5+} dopant and protons. The repulsion is clearly shown by the ab initio molecular dynamics simulations.

Introduction

Solid oxide fuel cells (SOFCs) are high-efficiency power generation devices and considered as a promising alternative to mitigate the energy and environmental issues associated with fossil fuel technologies.[1,2,3,4,5] The reduction of the operating temperature compared to conventional SOFCs based on yttria stabilized zirconia (YSZ) electrolytes can significantly reduce manufacturing and operating costs and increase the SOFC market penetration.[6] It is known that proton (H^+) conductors generally exhibit higher conductivity than oxide-ion (O^{2-}) conductors at low and intermediate temperatures (50–500 °C).[7,8,9,10,11,12,13,14,15] Therefore, protonic ceramic fuel cells (PCFCs) have recently attracted attention as a technology alternative to SOFCs.[7,8,9,10] To develop high-performance PCFCs for long-term use, high proton conductivity and high chemical stability of proton-conducting electrolytes are required.[16] Therefore, it is necessary to discover materials that exhibit high proton conductivity and chemical stability at low and intermediate temperatures.

Many polymer, hydrate, and salt materials are known as high proton conductors at low temperatures (50–200 °C), but, decompose at intermediate temperatures (200–500 °C).[17,18,19] For example, CsH_2PO_4 exhibits high proton conductivity from 230 to 254 °C, but decomposes above 254 °C.[17] In contrast, the oxides generally exhibit high chemical stability, but low proton conductivity at low and intermediate temperatures. As a result, there are no ionic conductors with both high ionic conductivity and high chemical stability within the "Norby gap", although the lack of suitable materials has stimulated the search for new ionic conductors.[15] Perovskite-type oxides (e.g., $BaCeO_3$- and $BaZrO_3$-based materials) are representative proton conductors.[14,20,21,22,23,24,25,26,27,28,29,30,31,32] Proton trapping is a major problem of these conventional perovskite-type proton conductors as follows.[15,33] The conventional strategy to enhance the proton conductivity is the acceptor M^{3+} doping into $Ba^{2+}B^{4+}O_3$ perovskite, $BaB_{1-x}M_xO_{3-\delta}$. Here, the acceptor is the dopant cation M with a lower valence than the host cation B, x is the dopant concentration, and the δ is the amount of oxygen vacancies in $BaB_{1-x}M_xO_{3-\delta}$. Proton conduction is facilitated by the hydration, which forms the proton H^+ in $BaB_{1-x}M_xO_{3-\delta+y/2}H_y$ (y: proton concentration). However, the proton H^+ is trapped by the M^{3+} with an effective negative charge of −1 compared to the B^{4+} due to the electrostatic attraction. This proton trapping could lead to proton-dopant cation association, higher apparent activation energy for proton conductivity, and lower proton conductivity at low and intermediate temperatures.[15,33] The low proton concentration y can be another major problem of the conventional perovskite-type proton conductors due to the amount of oxygen vacancies δ (e.g., y = 0.08 and δ = 0.05 in $BaCe_{0.9}Y_{0.1}O_{2.95}$), which leads to low proton conductivity.[33]

Recently, proton-conducting oxides with "intrinsic oxygen vacancies" have attracted much attention.[15,33,34,35,36,37,38,39,40,41,42,43,44,45,46,47,48,49,50,51,52,53] Here, the "intrinsic oxygen vacancies" v are the oxygen vacancies in a parent material (e.g., v in high temperature cubic Bi_2O_3).[54] The oxides with intrinsic oxygen vacancies v, such as $BaScO_{2.5}v_{0.5}$, enable the donor doping. The M^{n+}-donor doped $BaScO_{2.5}$ can be described as $BaSc_{1-x}M^{n+}{}_xO_{3-\delta}$. Here, M^{n+} is the donor dopant with a higher oxidation number than the host cation, n is the oxidation number of the M^{n+} cation and x is the dopant concentration.

In contrast to the conventional acceptor doping, the "donor doping into the oxides with intrinsic oxygen vacancies" could

[a] Department of Chemistry, School of Science, Institute of Science Tokyo, 2-12-1-W4-17, O-okayama, Meguro-ku, Tokyo 152-8551, Japan
[b] Institute of Materials Structure Science, High Energy Accelerator Research Organization (KEK), 1-1 Oho, Tsukuba, Ibaraki 305-0801, Japan
[c] J-PARC Center, High Energy Accelerator Research Organization (KEK), Tokai, Ibaraki, 319-1106, Japan

Supplementary Information available: [details of any supplementary information available should be included here]. See DOI: 10.1039/x0xx00000x

reduce the proton trapping due to the electrostatic repulsion between the proton and the donor dopant with the effective positive charge (e.g., the effective charge of Mo^{6+} at the Sc^{3+} site = +3).[15] Very recently, Saito and Yashima demonstrated high proton conductivity of Mo^{6+}-donor doped $BaScO_{2.5}$, $BaSc_{0.8}Mo_{0.2}O_{2.8}$ (n = 6).[15,55] Subsequently, Saito et al. reported higher proton conductivity of W^{6+}-donor doped $BaScO_{2.5}$, $BaSc_{0.8}W_{0.2}O_{2.8}$ (n = 6) than that of Mo^{6+}-donor doped $BaScO_{2.5}$.[33] The reduced proton trapping in donor-doped $BaScO_{2.5}$ leads to the low activation energy for the proton conductivity and high proton conductivity at low and intermediate temperatures.[15,33] In addition, donor doping into $BaScO_{2.5}$ can stabilize the cubic perovskite phase, although it is not an equilibrium phase in $BaScO_{2.5}$.[15] Hyodo et al. reported the proton conductivity of heavily Sc^{3+}-acceptor substituted $BaZrO_3$, $BaZr_{0.4}Sc_{0.6}O_{2.7}$ ($BaZr_{1-x}Sc_xO_{3-x/2}$; x = 0.6).[10] The heavily Sc-doped $BaZrO_3$ can be considered as Zr^{4+}-donor doped $BaScO_{2.5}$, $BaSc_{0.6}Zr_{0.4}O_{2.7}$ ($BaSc_{1-x}Zr_xO_{2.5+x/2}$; n = 4 and x = 0.4), because the Sc concentration 0.6 is higher than the Zr concentration 0.4. However, Hyodo et al. did not consider $BaZr_{0.4}Sc_{0.6}O_{2.7}$ as the Zr^{4+}-donor-doped $BaScO_{2.5}$, but as heavily Sc-doped $BaZrO_3$. As described above, $BaSc_{1-x}M^{n+}{}_xO_{3-\delta}$ (n = 6 and 4) have been reported, to the best of our knowledge, $BaSc_{1-x}M^{n+}{}_xO_{3-\delta}$ (n = 5) has not been reported in the literature. Herein, we report the high proton conductivity (e.g., 0.01 S cm^{-1} at 320 °C) in novel Nb^{5+}-donor-doped $BaScO_{2.5}$ ($BaSc_{1-x}Nb_xO_{2.5+x}$). In this work, we chose the compositions $BaSc_{1-x}Nb_xO_{2.5+x}$, because (i) donor-doped $BaScO_{2.5}$ materials exhibit high proton conductivity, (ii) Nb^{5+} can be a donor dopant as well as Mo^{6+} and W^{6+}, (iii) the ionic radius of Nb^{5+} (0.64 Å in 6-fold coordination) is larger than those of Mo^{6+} (0.59 Å in 6-fold coordination) and W^{6+} (0.60 Å in 6-fold coordination),[56] which could result in both high proton concentration and high proton conductivity,[33] and (iv) Nb-containing oxides such as $LaNbO_4$ exhibit high proton conductivity.[57]

Results and Discussions

White samples of novel oxides $BaSc_{1-x}Nb_xO_{2.5+x-y/2}(OH)_y$ (x = 0.20, 0.25, 0.35, 0.45) were synthesized by the solid-state reactions where the x is the Nb content and y is the proton concentration (See the details in the Methods Section in ESI). X-ray powder diffraction (XRD) measurements showed that the as-prepared sample of $BaSc_{0.8}Nb_{0.2}O_{2.7-y/2}(OH)_y$ (x = 0.20; BSN20) consists of the main cubic perovskite phase in addition to a small amount of impurity phase $Ba_3Sc_4O_9$ (**Fig. S1**). Meanwhile, all the reflections in the XRD patterns of as-prepared samples of $BaSc_{0.75}Nb_{0.25}O_{2.75-y/2}(OH)_y$ (x = 0.25; BSN25), $BaSc_{0.65}Nb_{0.35}O_{2.85-y/2}(OH)_y$ (x = 0.35; BSN35), and $BaSc_{0.55}Nb_{0.45}O_{2.95-y/2}(OH)_y$ (x = 0.45; BSN45) compositions were indexed by a primitive cubic lattice, indicating these samples to be a single cubic perovskite phase. To investigate the bulk conductivities σ_b of BSN25, BSN35, and BSN45, impedance measurements were performed. Typical impedance spectra in wet air of BSN25 at 46 °C are shown in **Fig. 1a**, which shows two semi-circles due to the bulk and grain boundary (gb) responses. To determine the bulk and gb conductivities, the equivalent circuit analyses were performed employing the models shown in **Fig. S2**. Reasonable fitting results were obtained (**Fig. S3**), Kramers–Kronig (KK) residuals were small (**Fig. S4**), and capacitance values were reasonable (**Table S1**), validating the impedance data and equivalent circuit analyses. BSN25 exhibited higher σ_b than the gb conductivity (**Fig. S5**). The σ_b of BSN25 was higher than those of BSN35 and BSN45 (**Fig. S6**). Therefore, we mainly focused on BSN25 for further studies.

To demonstrate the proton conduction in BSN25, H/D isotope exchange experiments were performed in D_2O-saturated air (D_2O/air) and H_2O-saturated air (H_2O/air) at 320 °C. The direct current (DC) electrical conductivity σ_{DC} showed a decrease from $\sigma_{DC}(H_2O)$ to $\sigma_{DC}(D_2O)$, when the atmosphere was changed from H_2O/air to D_2O/air (**Fig. S7a**). Here, the $\sigma_{DC}(H_2O)$ and $\sigma_{DC}(D_2O)$ represent the DC electrical conductivity in H_2O/air and D_2O/air, respectively. The $\sigma_{DC}(H_2O)/\sigma_{DC}(D_2O)$ ratio (1.6) was close to the value (1.4) from the classical theory.[58] The σ_{DC} was almost independent of the oxygen partial pressure $P(O_2)$ in the wide $P(O_2)$ range between 3 × 10^{-21} and 1 atm at 100 and 300 °C under wet conditions (water vapor partial pressure $P(H_2O)$ = 0.02 atm), indicating high chemical and electrical stability and suggesting ionic conduction (**Fig. S7b**). The bulk conductivity of BSN25 in wet air σ_{wet} was much higher than that in dry air σ_{dry} (**Fig. S8a**; e.g., σ_{wet} = 2800 σ_{dry} at 193 °C), indicating that the apparent transport number ($\sigma_{wet} - \sigma_{dry}$)/$\sigma_{wet}$ is close to unity (**Fig. S8b**). These results indicate that protons are the dominant conducting species in BSN25.

It should be noted that BSN25 exhibited high σ_b within the "Norby gap"[59] (e.g., 10^{-2} S cm^{-1} at 320 °C) and one of the highest proton conductivities among the ceramic proton conductors below 200 °C (**Fig. 1b**). BSN25 exhibited 12 times higher σ_b than that of $BaZr_{0.8}Y_{0.2}O_{2.9-y/2}(OH)_y$ (BZY; Ref. [60]) at 130 °C and 59 times higher σ_b than that of $BaCe_{0.9}Y_{0.1}O_{2.95-y/2}(OH)_y$ (BCY; Ref. [22]) at 230 °C. The higher σ_b of BSN25 compared to BCY and BZY is attributable to the higher proton concentration y and the higher proton diffusion coefficient D, as discussed below. BSN25

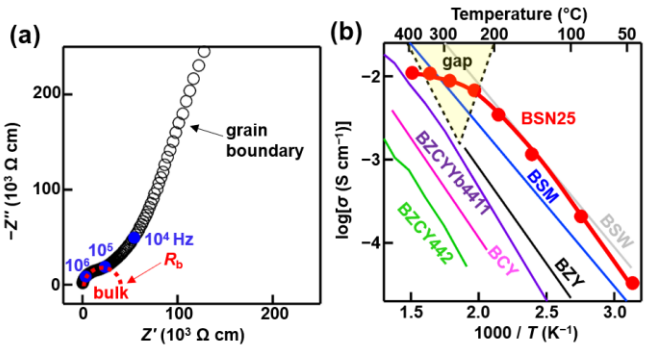

Fig. 1. (a) Complex impedance plots of $BaSc_{0.75}Nb_{0.25}O_{2.75-y/2}(OH)_y$ (BSN25) at 46 °C recorded in wet air. The red dotted high frequency semi-circle represents the bulk response. R_b denotes the bulk resistance. (b) "Norby gap", Arrhenius plots of bulk conductivity of BSN25, $BaSc_{0.8}Mo_{0.2}O_{2.8-y/2}(OH)_y$ (BSM),[15] $BaSc_{0.8}W_{0.2}O_{2.8-y/2}(OH)_y$ (BSW),[33] $BaZr_{0.8}Y_{0.2}O_{2.9-y/2}(OH)_y$ (BZY),[60] $BaCe_{0.9}Y_{0.1}O_{2.95-y/2}(OH)_y$ (BCY),[22] and $BaZr_{0.4}Ce_{0.4}Y_{0.1}Yb_{0.1}O_{2.9-y/2}(OH)_y$ (BZCYYb4411),[13] and Arrhenius plots of total AC conductivity of $BaZr_{0.4}Ce_{0.4}Y_{0.2}O_{2.9-y/2}(OH)_y$ (BZCY442)[63] under wet atmospheres.

showed 3 times higher σ_b than that of $BaSc_{0.8}Mo_{0.2}O_{2.8-y/2}(OH)_y$ (BSM; Ref. [15]) at 130 °C. The higher σ_b of BSN25 compared to BSM can be attributed to the higher y of BSN25 compared to BSM. Electrochemical devices such as PCFCs require high chemical stability of proton-conducting electrolytes for long-term use. To investigate the chemical stability of BSN25 in CO_2, BSN25 powders were annealed under CO_2 flow at 320 °C for 24 h. No significant difference was observed between the XRD patterns before and after annealing, indicating the high chemical stability of BSN25 against CO_2 (**Fig. 2a,d**). High chemical stability of BSN25 was also confirmed in dry H_2 and dry O_2 flow at 320 °C and wet CO_2 ($P(H_2O)$ = 0.02 atm) at room temperature for 24 h (**Fig. 2b,c,d** and **Fig. S9**). These high chemical stabilities, high proton transport number (**Fig. S8b**), high chemical and electrical stability (**Fig. S7b**), and high proton conductivity (= 0.011 >> 0.001 S cm^{-1} at 400 °C, **Fig. 1b**) indicate that BSN25 is a superior proton conductor.

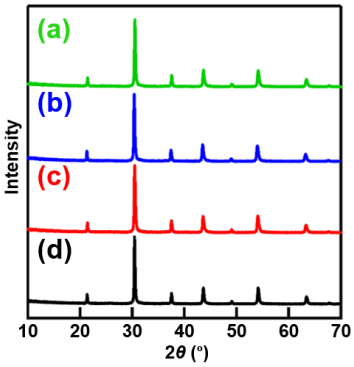

Fig. 2. Cu Kα X-ray powder diffraction patterns of BSN25 after annealing at 320 °C under (a) CO_2, (b) O_2, and (c) H_2 for 24 h and (d) before annealing.

Next, we discuss the reasons for the high bulk proton conductivity σ_b of BSN25. The σ_b is proportional to the proton concentration y and the proton diffusion coefficient D in bulk BSN25: $\sigma_b \propto y \times D$. To investigate the y and hydration of BSN25, thermogravimetric-mass spectrometric (TG-MS) and TG measurements were performed. The TG-MS results showed that the dehydration was the main cause of the weight loss upon heating (**Fig. 3**). Therefore, the y could be estimated from

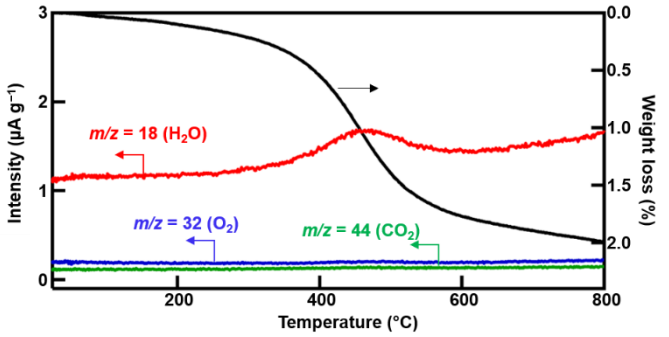

Fig. 3. Thermogravimetric-mass spectrometric (TG-MS) data of wet BSN25 powders measured under dry He flow. The sample weight decreased during heating. TG-MS data showed that the weight loss was mainly due to the dehydration (water evaporation, m/z = 18, red line). O_2 (m/z = 32, blue line) and CO_2 (m/z = 44, green line) from the sample were not detected.

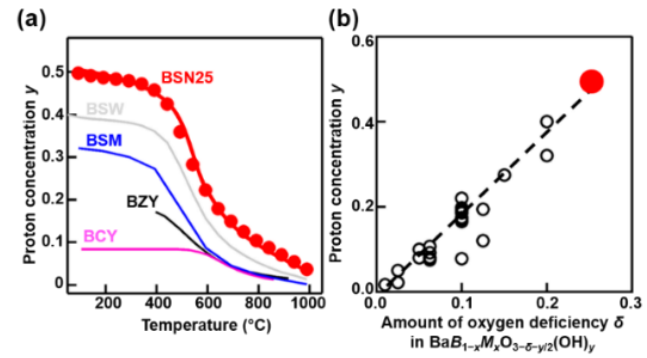

Fig. 4. (a) Temperature dependence of the proton concentration y in $BaB_{1-x}M_xO_{3-\delta-y/2}(OH)_y$ (red circles and curve: $BaSc_{0.75}Nb_{0.25}O_{2.75-y/2}(OH)_y$ (BSN25) [this work], black curve: BZY,[61] pink curve: BCY,[22] blue curve: BSM[15], and grey curve: BSW[33]), which were obtained by TG measurements. (b) Correlation between the amount of oxygen vacancies δ and y in $BaB_{1-x}M_xO_{3-\delta-y/2}(OH)_y$.[15,22,33,64,65] Red closed circle stands for the data of BSN25.

the weight change in the TG curve. The TG data showed the typical behavior of hydration with higher proton concentration at lower temperatures (**Fig. S10**). The proton concentration y of BSN25 (e.g., y = 0.50 at 100 °C and y = 0.46 at 400 °C) was higher than those of BSM (e.g., y = 0.32 at 100 °C)[15], BCY (e.g., y = 0.08 at 100 °C)[22], BZY (e.g., y = 0.17 at 400 °C)[61], and $BaSc_{0.8}W_{0.2}O_{2.8-y/2}(OH)_y$ (BSW; e.g., y = 0.40 at 100 °C)[33] (**Fig. 4a**). The higher y in BSN25 is a reason for its higher proton conductivity compared to BSM, BCY, and BZY. The y in hydrated perovskite ($BaB_{1-x}M_xO_{3-\delta-y/2}(OH)_y$) increases with increasing the amount of oxygen vacancies δ in $BaB_{1-x}M_xO_{3-\delta}$ without water (**Fig. 4b**). Therefore, the higher y in BSN25 is due to the larger amount of oxygen vacancies δ = 0.25 in BSN25 without water than those in BCY (δ = 0.05) and BZY (δ = 0.1). As described above, the bulk conductivity σ_b of BSN25 was higher than those of BSN35 and BSN45. The higher σ_b of BSN25 was attributable to the larger amount of oxygen vacancies of BSN25 (δ = 0.25) than those of BSN35 (δ = 0.15) and BSN45 (δ = 0.05), resulting in the higher proton concentration of BSN25. These results indicate that one reason for the high proton conductivity in BSN25 is the large amount of oxygen vacancies δ = 0.25 in BSN25 without water.

To investigate the bulk hydration and proton concentration of BSN25, we performed the Rietveld analyses of the neutron

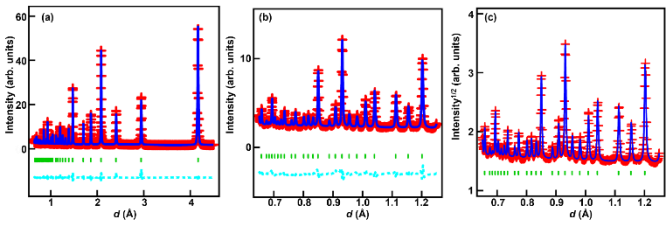

Fig. 5. Rietveld patterns of ND data of BSN25 in the d ranges of (a) 0.65–4.50 Å and (b,c) 0.65–1.25 Å, which were taken at −243 °C. Blue lines and red crosses are calculated and observed intensities, respectively. Green vertical bars denote calculated Bragg peak positions of cubic $Pm\bar{3}m$ BSN25. (a,b) The light blue dashed line is the difference pattern. (c) Vertical axis is the square root of the intensity.

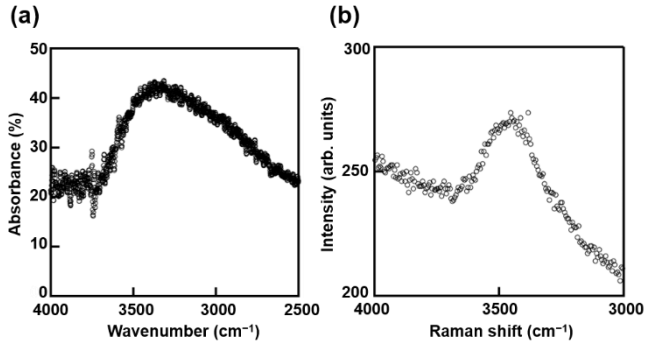

Fig. 6. (a) IR and (b) Raman spectra of wet BSN25 powders. We calculated OH bond length in BSN25 using an empirical equation to express the correlation between OH bond length and frequency using data of 21 materials.[66] The calculated OH bond length estimated from the infrared (IR) spectra (0.99(6) Å) and Raman spectra (0.98(6) Å) agreed with the OD bond length calculated for the refined average structure (**Fig. 7a**) and obtained by the pair distribution function (PDF) data (0.96 Å) (**Fig. S13**) of hydrated (deuterated) BSN25.

diffraction data of hydrated (deuterated) BSN25 (= $BaSc_{0.75}Nb_{0.25}O_{2.75-y/2}(OD)_y$ = $BaSc_{0.75}Nb_{0.25}O_{2.75}\cdot(y/2)\ D_2O$) at −243 °C. The calculated intensities based on the cubic $Pm\bar{3}m$ perovskite-type structure were in good agreement with the observed ones (**Fig. 5**), yielding reasonably small reliability factors (R_{wp} = 6.15%, R_B = 2.79%, R_F = 4.67%; **Table S2**). The refined lattice parameter of BSN25 (4.165220(3) Å) agreed with that optimized by the DFT calculations (4.22 Å). The refined atomic coordinates of the D atom in BSN25 were in agreement with those of $BaSc_{0.8}Mo_{0.2}O_{2.8-y/2}(OD)_y$ and optimized by the DFT calculations (**Table S3**). The OD bond length calculated for the refined structure of BSN25 (0.9999(17) Å) agreed with the OH bond lengths estimated from the infrared (IR) spectra (0.99(6) Å) and Raman scattering data (0.98(6) Å) (**Fig. 6**) and from the optimized structure by DFT calculations (1.000(11) Å) within one estimated standard deviation. These results indicate the formation of hydroxide ions OH in $BaSc_{0.75}Nb_{0.25}O_{2.75-y/2}(OH)_y$ and OD in $BaSc_{0.75}Nb_{0.25}O_{2.75-y/2}(OD)_y$. The bond valence sums

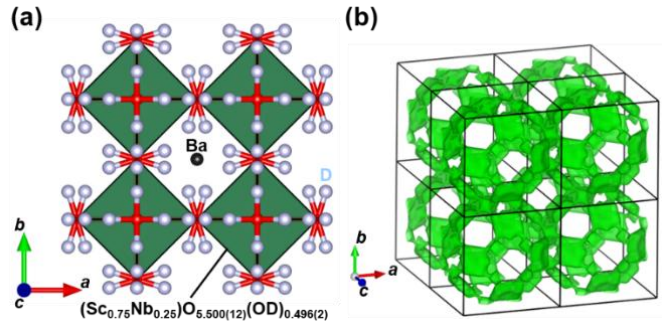

Fig. 7. (a) Refined crystal structure of $BaSc_{0.75}Nb_{0.25}O_3D_{0.5}$ (BSN25) at −243 ˚C, which was represented using $(Sc_{0.75}Nb_{0.25})O_{5.500(12)}(OD)_{0.496(2)}$ octahedra. Ba, O, and D atoms are denoted by the black, red, and grey spheres, respectively. The red/grey lines denote the OD bonds. The isotropic displacement spheres of Ba, O, and D atoms are plotted at the 60% probability level. (b) Isosurface of the bond-valence-based energy at 0.45 eV for a test proton of BSN25, which were calculated for the crystal parameters refined using the neutron diffraction data of BSN25 at −243 ˚C. Energy barrier for proton migration was estimated to be 0.38 eV, which agreed with the experimental activation energy for bulk diffusion coefficient 0.44 eV. Black square denotes a unit cell.

(BVSs) for Ba atom (2.0) and O atom (2.1) were in good agreement with their formal charges (**Table S2**). The average BVS of the cations at Sc/Nb site (3.2) was consistent with the average oxidation number (3.5). The BVS (0.8) for defective D atom was also consistent with its formal charge. These results validate the refined crystal structure of BSN25 (**Fig. 7a**). It should be noted that the refined occupancy factor of the O atom (0.9995(4)) agreed with the full occupation of O atoms at the O site (1.0000) within 2 times estimated standard deviation. In addition, the proton (deuteron) concentration y calculated from the refined occupancy factor of D atom y = 0.496(2) in bulk $BaSc_{0.75}Nb_{0.25}D_yO_{2.8+y/2}$ agreed with the value obtained from TG data y = 0.50 within 2 times standard deviation. Therefore, these structural and TG analyses indicated that the chemical formula of bulk BSN25 was $BaSc_{0.75}Nb_{0.25}O_{2.9982(12)}D_{0.496(2)}$ and water D_2O is fully incorporated as OD ions in bulk BSN25, leading to high proton concentration and high proton conductivity of BSN25. Namely, the fractional water uptake F_w of hydrated BSN25 was 100% and its chemical formula was $BaSc_{0.75}Nb_{0.25}O_3D_{0.5}$. Here, we define the fractional water uptake F_w as $F_w = y/2\delta$. Full hydration is an important factor for high proton conductivity. **Fig. 7b** shows the isosurface of bond-valence-based energy landscape of BSN25, indicating the three-

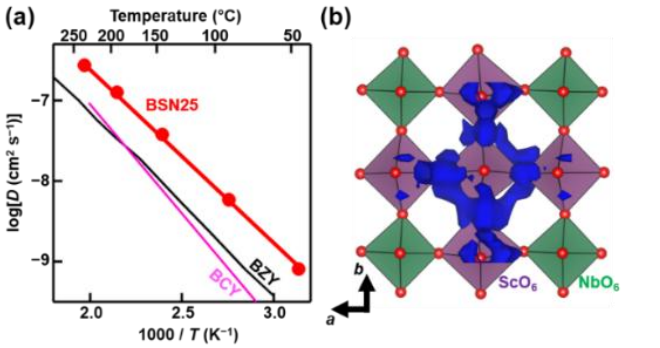

Fig. 8. (a) Arrhenius plots of experimental bulk proton diffusion coefficient D of $BaSc_{0.75}Nb_{0.25}O_{2.75-y/2}(OH)_y$ (BSN25) (red circles and line), BZY (black line),[61] and BCY (pink line).[62] (b) Blue isosurface of the proton probability density at 0.005 Å^{-3} in $Ba_8Sc_6Nb_2O_{24}H_4$ viewed along the c axis from the AIMD simulations at 1500 ˚C ($-0.05 \le x \le 1.05$; $-0.05 \le y \le 1.05$; $-0.3 \le z \le 0.05$). Each red sphere represents an O atom. The green and purple squares denote NbO_6 and ScO_6 octahedra, respectively.

dimensional network of proton diffusion pathways.

Next, we discuss the bulk proton diffusion coefficient D of BSN25. The experimental D was estimated using the Nernst-Einstein equation:

$D = \sigma_b RT/F^2y$ (1)

where σ_b is the bulk conductivity, R is gas constant, T is absolute temperature, F is Faraday constant, and y is proton concentration obtained by the TG measurements. The D of BSN25 was higher than those of BZY and BCY (**Fig. 8a**). From Eq. (1), the bulk conductivity σ_b is expressed as $\sigma_b = DF^2y/RT$. Since both D and y of BSN25 are high (**Figs. 4a,b** and **8a**), the σ_b of BSN25 is higher than σ_b of other proton conductors.

Next, we discuss the origin of high D of BSN25. The activation energy E_a for D of the present Nb-donor-doped $BaScO_{2.5}$ (BSN25) was estimated to be 0.44 eV, which was close to that

of the Mo-donor-doped $BaScO_{2.5}$ (BSM) (0.41 eV)[15] and W-donor-doped $BaScO_{2.5}$ (BSW) (0.43 eV)[33] and lower than those of the acceptor-doped proton conductors such as BZY (0.48 eV)[61] and BCY (0.54 eV)[62] at low temperatures of 50–170 °C. The low E_a of BSN25 suggests the reduced proton trapping, due to the repulsion between the donor dopant and proton, as well as the E_a of BSM and BSW.[15,33] To show the repulsion between the Nb donor dopant and protons, the probability density distribution of protons in $Ba_8Sc_6Nb_2O_{24}H_4$ (= $[BaSc_{0.75}Nb_{0.25}O_3H_{0.5}]_8$) was investigated by the ab initio molecular dynamics (AIMD) simulations (**Fig. 8b**). AIMD simulations were performed for the 2 × 2 × 2 supercell $Ba_8Sc_6Nb_2O_{24}H_4$ (= $[BaSc_{0.75}Nb_{0.25}O_3H_{0.5}]_8$) (see the details in Methods Section in ESI). It should be noted that the protons are not near the oxide ions coordinated to a Nb cation but to a Sc cation, indicating that the protons migrate around the ScO_6 octahedra while avoiding the NbO_6 octahedra (**Fig. 8b**). This result clearly indicates the repulsion between the Nb donor dopant and protons, supporting the reduced proton trapping.

Conclusions

In conclusion, we prepared the pentavalent donor-doped $BaScO_{2.5}$ perovskite for the first time. We have demonstrated that the $BaSc_{0.75}Nb_{0.25}O_{2.75-y/2}(OH)_y$ (BSN25) perovskite exhibits one of the highest proton conductivities among the ceramic proton conductors below 200 °C. The high proton conductivity of BSN25 is attributable to its high concentration and diffusion coefficient of protons. The high proton concentration is ascribed to high oxygen vacancy concentration in BSN25 without water. The high proton diffusion coefficient D at low and intermediate temperatures can be attributed to the low activation energy E_a for D (0.44 eV). The low E_a suggests the reduced proton trapping due to the repulsion between the donor Nb^{5+} dopant and protons. The repulsion was clearly shown by the AIMD simulations. These findings would accelerate the development of the innovative proton conductors based on the novel strategy, “donor doping into the oxides with intrinsic oxygen vacancies”.

Author contributions

M.Y. and K.S. designed research project. M.B. and K.U. prepared the samples, performed the TG, TG-MS, and XRD measurements and measured transport properties. K.S. performed Rietveld analysis of neutron diffraction data, BVEL calculations, and DFT calculations. K.F. and T.H. performed neutron diffraction measurement. K.S. and M.Y. wrote and edited original manuscript. M.Y. supervised the research and conceived the project. Main funding acquisition: M.Y. and K.F. All authors read the manuscript. K.S., M.B., and K.U. contributed equally to this work.

Conflicts of interest

There are no conflicts to declare.

Data availability

The data supporting this article are included as part of the ESI.†

Acknowledgements

We acknowledge Dr. Y. Sakuda and Mr. R. Maeda for their help in experiments and valuable discussions. We express special thanks to Shin-Etsu Chemical Co., Ltd. and Kojundo Chemical Laboratory Co., Ltd. for providing raw materials. We express special thanks to Ms. K. Suda of the Materials Analysis Division, Open Facility Center, Tokyo Institute of Technology for the TG-MS measurements. We also acknowledge Prof. S. Ito and Dr. M. Tada for performing IR and Raman measurements, respectively. We performed neutron diffraction measurements by the project approval (JRR-3 Proposal Nos. 24609; J-PARC: Proposal Nos. 2024A0178 and 2020L0804). This work was supported by Grant-in-Aid for Scientific Research (KAKENHI, JP21K18182, JP23K04887, JP23H04618, and JP24H00041) from the Ministry of Education, Culture, Sports, Science, and Technology of Japan, Adopting Sustainable Partnerships for Innovative Research Ecosystem (ASPIRE) from the Japan Science and Technology Agency (JST) (Grant JPMJAP2308), the Adaptable and Seamless Technology Transfer Program through Target-Driven R&D (A-STEP) from JST (Grant JPMJTR22TC), the Institute for Solid State Physics, the University of Tokyo, and the Center of Neutron Science for Advanced Materials, Institute for Materials Research, Tohoku University. K.S. acknowledges support from a JSPS Fellowship for Young Scientists, DC1 (23KJ0953).

Notes and references

1 K. Develos-Bagarinao, T. Ishiyama, H. Kishimoto, H. Shimada and K. Yamaji, Nanoengineering of cathode layers for solid oxide fuel cells to achieve superior power densities, *Nat. Commun.*, 2021, **12**, 3979.

2 B. C. H. Steele and A. Heinzel, Materials for fuel-cell technologies, *Nature*, 2001, **414**, 345–352.

3 T. Ishihara, H. Matsuda and Y. Takita, Doped $LaGaO_3$ perovskite type oxide as a new oxide ionic conductor, *J. Am. Chem. Soc.*, 1994, **116**, 3801–3803.

4 S. J. Skinner and J. A. Kilner, Oxygen diffusion and surface exchange in $La_{2-x}Sr_xNiO_{4+\delta}$, *Solid State Ionics*, 2000, **135**, 709–712.

5 M. Yashima, T. Tsujiguchi, Y. Sakuda, Y. Yasui, Y. Zhou, K. Fujii, S. Torii, T. Kamiyama and S. J. Skinner, High oxide-ion conductivity through the interstitial oxygen site in $Ba_7Nb_4MoO_{20}$-based hexagonal perovskite related oxides, *Nat. Commun.*, 2021, **12**, 556.

6 E. Fabbri, L. Bi, D. Pergolesi and E. Traversa, High-performance composite cathodes with tailored mixed conductivity for intermediate temperature solid oxide fuel cells using proton conducting electrolytes, *Energy Environ. Sci.*, 2011, **4**, 4984–4993.

7 T. Norby, The promise of protonics, *Nature*, 2001, **410**, 877–878.

8 W. Bian, W. Wu, B. Wang, W. Tang, M. Zhou, C. Jin, H. Ding, W. Fan, Y. Dong, J. Li and D. Ding, Revitalizing interface in protonic ceramic cells by acid etch, *Nature*, 2022, **604**, 479–485.

9 K. Jiao, J. Xuan, Q. Du, Z. Bao, B. Xie, B. Wang, Y. Zhao, L. Fan, H. Wang, Z. Hou, S. Huo, N. P. Brandon, Y. Yin and M. D. Guiver, Designing the next generation of proton-exchange membrane fuel cells, *Nature*, 2021, **595**, 361–369.

10 J. Hyodo, K. Kitabayashi, K. Hoshino, Y. Okuyama and Y. Yamazaki, Fast and stable proton conduction in heavily scandium-doped polycrystalline barium zirconate at intermediate temperatures, *Adv. Energy Mater.*, 2020, **10**, 2000213.

11 C. Xia, Y. Mi, B. Wang, B. Lin, G. Chen and B. Zhu, Shaping triple-conducting semiconductor $BaCo_{0.4}Fe_{0.4}Zr_{0.1}Y_{0.1}O_{3-\delta}$ into an electrolyte for low-temperature solid oxide fuel cells, *Nat. Commun.*, 2019, **10**, 1707.

12 C. Duan, J. Huang, N. Sullivan and R. O'Hayre, Proton-conducting oxides for energy conversion and storage, *Appl. Phys. Rev.*, 2020, **7**, 011314.

13 S. Choi, C. J. Kucharczyk, Y. Liang, X. Zhang, I. Takeuchi, H. Il Ji and S. M. Haile, Exceptional power density and stability at intermediate temperatures in protonic ceramic fuel cells, *Nat. Energy*, 2018, **3**, 202–210.

14 T. Chen, Y. Jing, L. O. Anderson, K. Leonard, H. Matsumoto, N. Aluru and N. H. Perry, Toward durable protonic ceramic cells: hydration-induced chemical expansion correlates with symmetry in the Y-doped $BaZrO_3$–$BaCeO_3$ solid solution, *J. Phys. Chem. C*, 2021, **125**, 26216–26228.

15 K. Saito and M. Yashima, High proton conductivity within the 'Norby gap' by stabilizing a perovskite with disordered intrinsic oxygen vacancies, *Nat. Commun.*, 2023, **14**, 7466.

16 S. Guo, L. Jiang, Y. Li, P. Zhong, S. A. Ismail and T. Norby, From electrolyte and electrode materials to large-area protonic ceramic fuel cells: a review, *Adv. Func. Mater.*, 2024, **34**, 2304729.

17 S. M. Haile, C. R. I. Chisholm, K. Sasaki, D. A. Boysen and T. Uda, Solid acid proton conductors: from laboratory curiosities to fuel cell electrolytes, *Faraday Discuss.*, 2007, **134**, 17–39.

18 M. Nagao, T. Kamiya, P. Heo, A. Tomita, T. Hibino and M. Sano, Proton conduction in In^{3+}-doped SnP_2O_7 at intermediate temperatures, *J. Electrochem. Soc.*, 2006, **153**, A1604–A1609.

19 S. R. Phadke, C. R. Bowers, E. D. Wachsman and J. C. Nino, Proton conduction in acceptor doped SnP_2O_7, *Solid State Ionics*, 2011, **183**, 26–31.

20 P. A. Stuart, T. Unno, J. A. Kilner and S. J. Skinner, Solid oxide proton conducting steam electrolysers, *Solid State Ionics*, 2008, **179**, 1120–1124.

21 H. Iwahara, T. Yajima, T. Hibino, K. Ozaki and H. Suzuki, Protonic conduction in calcium, strontium and barium zirconates, *Solid State Ionics*, 1993, **61**, 65–69.

22 K. D. Kreuer, Proton-conducting oxides, *Annu. Rev. Mater. Res.*, 2003, **33**, 333–359.

23 C. Kjølseth, L. Y. Wang, R. Haugsrud and T. Norby, Determination of the enthalpy of hydration of oxygen vacancies in Y-doped $BaZrO_3$ and $BaCeO_3$ by TG-DSC, *Solid State Ionics*, 2010, **181**, 1740–1745.

24 D. Han, K. Shinoda, S. Sato, M. Majima and T. Uda, Correlation between electroconductive and structural properties of proton conductive acceptor-doped barium zirconate, *J. Mater. Chem. A*, 2015, **3**, 1243–1250.

25 H. Takahashi, I. Yashima, K. Amezawa, K. Eguchi, H. Matsumoto, H. Takamura and S. Yamaguchi, First-principles calculations for the energetics of the hydration reaction of acceptor-doped $BaZrO_3$, *Chem. Mater.*, 2017, **29**, 1518–1526.

26 I. Oikawa, M. Ando, Y. Noda, K. Amezawa, H. Kiyono, T. Shimizu, M. Tansho and H. Maekawa, Defects in scandium doped barium zirconate studied by Sc-45 NMR, *Solid State Ionics*, 2011, **192**, 83–87.

27 Y. Ling, H. Chen, J. Niu, F. Wang, L. Zhao, X. Ou, T. Nakamura and K. Amezawa, Bismuth and indium co-doping strategy for developing stable and efficient barium zirconate-based proton conductors for high-performance H-SOFCs, *J. Eur. Ceram. Soc.*, 2016, **36**, 3423–3431.

28 I. Kosacki and H. L. Tuller, Mixed conductivity in $SrCe_{0.95}Yb_{0.05}O_3$ protonic conductors, *Solid State Ionics*, 1995, **80**, 223–229.

29 H. Kawamori, I. Oikawa and H. Takamura, Protonation-induced B-site deficiency in perovskite-type oxides: fully hydrated $BaSc_{0.67}O(OH)_2$ as a proton conductor, *Chem. Mater.*, 2021, **33**, 5935–5942.

30 K. Leonard, Y. Okuyama, Y. Takamura, Y. S. Lee, K. Miyazaki, M. E. Ivanova, W. A. Meulenberg and H. Matsumoto, Efficient intermediate-temperature steam electrolysis with Y : $SrZrO_3$–$SrCeO_3$ and Y : $BaZrO_3$–$BaCeO_3$ proton conducting perovskites, *J. Mater. Chem. A*, 2018, **6**, 19113–19124.

31 I. Oikawa and H. Takamura, Correlation among oxygen vacancies, protonic defects, and the acceptor dopant in Sc-doped $BaZrO_3$ studied by ^{45}Sc nuclear magnetic resonance, *Chem. Mater.*, 2015, **27**, 6660–6667.

32 K. Leonard, Y. S. Lee, Y. Okuyama, K. Miyazaki and H. Matsumoto, Influence of dopant levels on the hydration properties of SZCY and BZCY proton conducting ceramics for hydrogen production, *Int. J. Hydrogen Energy*, 2017, **42**, 3926–3937.

33 K. Saito, K. Umeda, K. Fujii, K. Mori and M. Yashima, High proton conduction by full hydration in highly oxygen deficient perovskite, *J. Mater. Chem. A*, 2024, **12**, 13310–13319.

34 C. A. Fuller, D. A. Blom, T. Vogt, I. R. Evans and J. S. O. Evans, Oxide ion and proton conductivity in a family of highly oxygen-deficient perovskite derivatives, *J. Am. Chem. Soc.*, 2021, **144**, 615–624.

35 Y. Youn, B. Hussain, A. Ullah, I. J. Hwang, J. Shin, J. Hong, D. W. Joh, S. Lee, R. Song, S. Park, T. W. Kim, Y. Choi, T. Lim and H. Kim, Anisotropic proton migration in hexagonal perovskite-related $Ba_5Er_2Al_2ZrO_{13}$ oxide, *Chem. Mater.*, 2023, **35**, 9493–9504.

36 C. A. Fuller, Q. Berrod, B. Frick, M. R. Johnson, M. Avdeev, J. S. O. Evans and I. R. Evans, Oxide ion and proton conductivity in highly oxygen-deficient cubic perovskite $SrSc_{0.3}Zn_{0.2}Ga_{0.5}O_{2.4}$, *Chem. Mater.*, 2020, **32**, 4347–4357.

37 C. A. Fuller, J. I. Murrell, D. A. Blom, T. Vogt, W. Zhang, P. S. Halasyamani, I. R. Evans and J. S. O. Evans, Oxide ion conductivity, proton conductivity, and phase transitions in

perovskite-derived $Ba_{3-x}Sr_xYGa_2O_{7.5}$ $0 \le x \le 3$ materials, *Chem. Mater.*, 2022, **34**, 3185–3196.

38 R. Andreev, D. Korona, I. Anokhina, I. Animitsa, Proton and oxygen-ion conductivities of hexagonal perovskite $Ba_5In_2Al_2ZrO_{13}$, *Materials*, 2022, **15**, 3944.

39 A. J. Brown, O. J. Wagstaff, I. R. Evans, J. S. O. Evans, R. A. Mole, J. Wykes, M. Avdeev and C. D. Ling, Distinct intercalation and conduction behaviors within an isostructural series $Ba_5R_2Al_2SnO_{13}$, *Chem. Mater.*, 2024, **36**, 8188–8198.

40 Y. Yasui, M. Tansho, K. Fujii, Y. Sakuda, A. Goto, S. Ohki, Y. Mogami, T. Iijima, S. Kobayashi, S. Kawaguchi, K. Osaka, K. Ikeda, T. Otomo and M. Yashima, Hidden chemical order in disordered $Ba_7Nb_4MoO_{20}$ revealed by resonant X-ray diffraction and solid-state NMR, *Nat. Commun.*, 2023, **14**, 2337.

41 T. Murakami, J. R. Hester and M. Yashima, High proton conductivity in $Ba_5Er_2Al_2ZrO_{13}$, a hexagonal perovskite-related oxide with intrinsically oxygen-deficient layers, *J. Am. Chem. Soc.*, 2020, **142**, 11653–11657.

42 T. Murakami, M. Avdeev, R. Morikawa, J. R. Hester and M. Yashima, High proton conductivity in β-Ba_2ScAlO_5 enabled by octahedral and intrinsically oxygen-deficient layers, *Adv. Func. Mater.* 2022, **33**, 2206777.

43 Y. Sakuda, T. Murakami, M. Avdeev, K. Fujii, Y. Yasui, J. R. Hester, M. Hagihala, Y. Ikeda, Y. Nambu and M. Yashima, Dimer-mediated cooperative mechanism of ultrafast-ion conduction in hexagonal perovskite-related oxides, *Chem. Mater.*, 2023, **35**, 9774–9788.

44 K. Saito, K. Fujii and M. Yashima, Oxide-ion and proton conductivity of the ordered perovskite $BaY_{1/3}Ga_{2/3}O_{2.5}$, *J. Solid State Chem.*, 2022, **306**, 122733.

45 R. Morikawa, T. Murakami, K. Fujii, Y. Nambu and M. Yashima, High proton conduction in Ba_2LuAlO_5 with highly oxygen-deficient layers, *Commun. Mater.*, 2023, **4**, 42.

46 K. Matsuzaki, K. Saito, Y. Ikeda, Y. Nambu and M. Yashima, High proton conduction in the octahedral layers of fully hydrated hexagonal perovskite-related oxides, *J. Am. Chem. Soc.*, 2024, 146, 18544–18555.

47 T. Schober, Protonic conduction in $BaIn_{0.5}Sn_{0.5}O_{2.75}$, *Solid State Ionics*, 1998, **109**, 1–11.

48 N. Hideshima and K. Hashizume, Effect of partial substitution of In by Zr, Ti and Hf on protonic conductivity of $BaInO_{2.5}$, *Solid State Ionics*, 2010, **181**, 1659–1664.

49 E. Quarez, S. Noirault, M. T. Caldes and O. Joubert, Water incorporation and proton conductivity in titanium substituted barium indate, *J. Power Sources*, 2010, **195**, 1136–1141.

50 A. Rolle, R. N. Vannier, N. V. Giridharan and F. Abraham, Structural and electrochemical characterization of new oxide ion conductors for oxygen generating systems and fuel cells, *Solid State Ionics*, 2005, **176**, 2095–2103.

51 A. Rolle, P. Roussel, N. V. Giridharan, E. Suard and R. N. Vannier, A neutron diffraction study of the oxygen diffusion in molybdenum doped $Ba_2In_2O_5$, *Solid State Ionics*, 2008, **179**, 1986–1995.

52 N. A. Tarasova, A. O. Galisheva, I. E. Animitsa and D. V. Korona, Hydration and the state of oxygen–hydrogen groups in the complex oxide $BaLaIn_{0.9}Nb_{0.1}O_{4.1}$ with the Ruddlesden–Popper structure, *Russ. J. Phys. Chem. A*, 2020, **94**, 818–821.

53 N. Tarasova, I. Animitsa, A. Galisheva and V. Pryakhina, Protonic transport in the new phases $BaLaIn_{0.9}M_{0.1}O_{4.05}$ (*M* = Ti, Zr) with Ruddlesden-Popper structure, *Solid State Sci.*, 2020, **101**, 106121.

54 M. Yashima and D. Ishimura, Crystal structure and disorder of the fast oxide-ion conductor cubic Bi_2O_3, *Chem. Phys. Lett.*,2003, **378**, 395–399.

55 K. Saito and M. Yashima, A novel fast proton conductor created by the donor doping into the oxide with intrinsic oxygen vacancies, *J. Fuel Cell Technol.*, 2024, **23**, 73.

56 R. D. Shannon, Revised effective ionic radii and systematic studies of interatomic distances in halides and chalcogenides, *Acta Crystallogr. A*, 1976, **32**, 751–767.

57 R. Haugsrud and T. Norby, Proton conduction in rare-earth ortho-niobates and ortho-tantalates, *Nat. Mater.*, 2006, **5**, 193–196.

58 A. S. Nowick and A. V. Vaysleyb, Isotope effect and proton hopping in high-temperature protonic conductors, *Solid State Ionics*, 1997, **97**, 17–26.

59 T. Norby, Solid-state protonic conductors: principles, properties, progress and prospects, *Solid State Ionics*, 1999, **125**, 1–11.

60 D. Han, N. Hatada, T. Uda and R. Koc, Chemical expansion of yttrium-doped barium zirconate and correlation with proton concentration and conductivity, *J. Am. Ceram. Soc.*, 2016, **99**, 3745–3753.

61 J. Lagaeva, D. Medvedev, A. Demin and P. Tsiakaras, Insights on thermal and transport features of $BaCe_{0.8-x}Zr_xY_{0.2}O_{3-\delta}$ proton-conducting materials, *J. Power Sources*, 2015, **278**, 436–444.

62 K. D. Kreuer, S. Adams, W. Münch, A. Fuchs, U. Klock and J. Maier, roton conducting alkaline earth zirconates and titanates for high drain electrochemical applications, *Solid State Ionics*, 2001, **145**, 295–306.

63 J. Hyodo, K. Tsujikawa, M. Shiga, Y. Okuyama and Y. Yamazaki, Accelerated discovery of proton-conducting perovskite oxide by capturing physicochemical fundamentals of hydration, *ACS Energy Lett.*, 2021, **6**, 2985–2992.

64 A. K. E. Andersson, S. M. Selbach, C. S. Knee and T. Grande, Chemical expansion due to hydration of proton-conducting perovskite oxide ceramics, *J. Am. Ceram. Soc.*, 2014, **97**, 2654–2661.

65 A. Novak, Hydrogen bonding in solids correlation of spectroscopic and crystallographic data. in Large Molecules, Springer, Berlin, Heidelberg, 1974; 177–216.

Data availability

The data supporting this article have been included as part of the ESI.†